Large-eddy simulation of ultra-high Atwood number Rayleigh-Taylor mixing using the nLES method

By G. C. Burton

1. Motivation and objective

Rayleigh-Taylor instability (RTI) occurs when a heavier fluid of density $\rho_{_H}$ sits atop a lighter fluid of density $\rho_{_L}$, with a gravitational field vector $\mathbf{g}$ aligned normal to the two-fluid interface and opposed to the density gradient (Rayleigh 1883; Taylor 1950). The flow is important to a variety of engineering and scientific applications, such as inertial confinement fusion (ICF), astrophysics, oceanography and meteorology. For ICF applications, turbulent mixing arising from RTI at the interfaces between capsule shells is directly related to decreasing thermonuclear (TN) yield during capsule implosion (Amendt *et al.* 2002). Similarly, RTI mixing during supernovae collapse directly influences the rate and efficiency of TN burn and the creation of heavy elements (Cabot & Cook 2006). In both ICF and astrophysical applications, Reynolds numbers can exceed $Re_h = 10^4$, and Atwood numbers, defined as $A \equiv (\rho_{_H} - \rho_{_L})/(\rho_{_H} + \rho_{_L})$, can exceed $A \geq 0.85$, with some astrophysical conditions approaching $A \to 1$, *i.e.,* a gas-vacuum interface. The growth rate of the RTI mixing layer, as well as the efficiency of that mixing, at high Reynolds and Atwood numbers are thus key issues in experimental and computational studies of RTI.

In most RTI flows, motion occurs first at the smallest dynamically significant scales, where perturbations at the density interface cause a misalignment of the pressure and density gradients, giving rise to baroclinic torque $\Gamma_{bar} \equiv \nabla\rho \times \nabla p$ that sets the system in motion. Heavy fluid falls as spikes into the lighter fluid, and the lighter fluid rises as bubbles into the heavy fluid due to buoyancy forces. This movement creates secondary Kelvin-Helmholtz instabilities (KHI) in the shear layers between individual structures and the local quiescent fluid. Both the RTI and KHI transfer kinetic and scalar energy from the small scales to successively larger scales in the system, through an *inverse cascade* process, *i.e.,* in a direction *opposed* to the usual forward cascade of Kolmogorov theory. As the bubbles and spikes grow, they begin to combine in a nonlinear fashion, due to the coupling between the buoyancy and inertial forces. At a later time, the RTI layer undergoes a mixing transition and becomes fully turbulent (Cook & Dimotakis 2001). Mixing layer dynamics then become dominated by vortex stretching and a *forward cascade* of kinetic and scalar energies, which drives the creation of smaller scales. Molecular mixing arising from the forward cascade reduces density gradients and thus the buoyancy forces within the mixing layer. At very late times and in finite domains, this process drives the system to a fully mixed, quiescent state.

Early analytical work by Chandrasekhar (1961) established that, for a single mode perturbation with amplitude h_o and wavelength $\lambda = 2\pi/k$, in the linear regime where $h \ll 1/k$, the amplitude grows exponentially as $h(t) = h_o \cosh(\gamma t)$. Here $\gamma \equiv \sqrt{Agk}$ is the growth rate and A is the Atwood number. For larger amplitudes, where $h > 1/k$,

nonlinear interactions between individual modes dominate the flow and alter the mixing layer growth rate. Numerous studies have shown that the asymptotic growth rate of the mixing layer in the nonlinear regime follows the relation $h_b = \alpha_b A g t^2$, where h_b is the bubble height, t is the time and α_b is the bubble growth constant, with a similar relation for the spikes, involving h_s and α_s. However, despite a half century of analytical, experimental and computational work, there is no agreement on the values of these growth constants, or their dependence on either the initial conditions or the Atwood number. Indeed, these issues have come to dominate many contemporary studies of RTI mixing (Glimm *et al.* 2001; Dimonte *et al.* 2004, 2005).

While numerous RTI studies have appeared in the literature, relatively few have addressed the high Atwood, high Reynolds-number regime that is important to certain engineering and scientific applications, as discussed above. Read (1984) presented a study of immiscible RT experiments with ethyl alcohol and air, at a density ratio of 600 : 1, *i.e.,* $A = 0.997$, and reported $\alpha_b \approx 0.074$, a value essentially unchanged from the lower Atwood-number findings of that study. Dimonte & Schneider (2000) also reported immiscible RTI experiments using SF_6 with butane and freon, at Atwood numbers between 0.92 and 0.96, that produced steady values of $\alpha_b \approx 0.046 - 0.052$. That study, and others, have also noted growing anisotropy of bubble and spike growth rates with increasing Atwood number. Indeed, Dimonte & Schneider found evidence that the ratio of growth rates scaled as $\alpha_s/\alpha_b \sim R^{D_\alpha}$, where $R \equiv \rho_{_H}/\rho_{_L}$ and where $D_\alpha \approx 0.33 \pm 0.05$ for $R \leq 50$. Other studies have developed analytical models based on potential-flow theory to predict bubble evolution of single-mode, classical Rayleigh-Taylor instability at very high Atwood numbers $A \rightarrow 1$ (Layzer 1955; Alon *et al.* 1995; Goncharov 2002; Sohn 2003; Mikaelian 2003). However, the extension of these analytical models to nonlinear growth of three-dimensional multimode RTI, of the sort seen in actual engineering applications, remains problematic.

Numerical studies of RTI mixing have appeared more frequently as computing power has grown in the past three decades. Simulations offer a complementary means to study RTI flows, as they permit precise introduction of initial conditions, and allow direct access to all time and length scales in the flow. Most of these studies, however, have examined only low or intermediate Atwood-number and Reynolds-number RTI configurations (Dimonte *et al.* 2004; Ramaprabhu *et al.* 2005). In addition, most have reported growth rates $\alpha_b \approx 0.02 - 0.03$, significantly smaller than experimental results in the same configurations. The cause of this disparity is currently the subject of much debate, but the behavior is consistent, at least in part, with overly dissipative numerical methods that overestimate molecular mixing, thereby unphysically reducing buoyancy and, ultimately, RTI growth rates.

With the advent of terascale computing, several high-resolution simulations of RTI flow have been produced in the past decade (Cook & Dimotakis 2001; Ristorcelli & Clark 2004). Some of these studies have explored the higher Reynolds-number regime $Re_h \geq 10^4$, and in so doing, have provided the first numerical examination of fully turbulent, nonlinear mixing-layer dynamics (Cook *et al.* 2004; Cabot & Cook 2006). However, such studies have remained limited to Atwood numbers $A \leq 0.5$. In addition, despite the higher resolution, and the consequent smaller impact of numerical dissipation, such studies have not reported increases in mixing-layer growth rates, as suggested by the experimental studies.

At the same time, very few large-eddy or direct numerical simulations have been conducted of multimode RTI turbulence in the nonlinear regime above $A > 0.7$ (Olson &

Cook 2007; Youngs 1991), and none appears to exist in the ultra-high Atwood regime above $A > 0.90$, where density differences may be significantly closer to conditions seen in many engineering and scientific applications. Indeed, the only reported multimode study of RTI at $A = 0.9$ is that of Youngs (1991) using implicit LES techniques. While such techniques have provided a useful tool for examining RTI and other flows (Grinstein *et al.*, 2007; Youngs 2009), most implicit LES methods use an artificial dissipation, built into the numerics through derivative upwinding, to keep the simulation stable and reasonably accurate. As a result, like virtually all other current LES methods, implicit LES techniques cannot recover the actual *two-way exchange of energy* arising from forward transfer and backscatter between the resolved and subgrid fields in a large-eddy simulation that is essential to the evolution of RTI and other buoyancy-driven flows. Furthermore, by introducing a nonphysical dissipation to the resolved scales, all such artificial dissipation methods may unphysically distort the smaller-resolved scales, which are most tightly coupled to the buoyancy-induced instabilities that are central to the evolution of RTI flows and mixing rates.

2. Numerical method

2.1. *The nLES method and Rayleigh-Taylor mixing*

Given the limitations of current numerical techniques, the goal of the present project is to extend the Nonlinear LES (nLES) method to simulations of ultra-high Atwood-number, high Reynolds-number Rayleigh-Taylor mixing. The nLES method represents a fundamental paradigm shift in turbulence modeling, away from artificial viscosity and other numerically dissipative LES methods that have, as discussed above, directly hampered numerical study of RTI mixing. The nLES method is the first LES technique that directly solves the nonlinear advective terms, *e.g.,* $\overline{\rho\, u_i\, u_j}$, appearing in the flow equations, and does so without the use of artificial viscosities, diffusivities or dealiasing. Indeed, with this strategy, the nLES method is the first technique that can directly capture the local instantaneous structure of *two-way* kinetic energy transfer – both forward transfer and backscatter – between the resolved and subgrid scales in an LES, with correlations exceeding $\rho \geq 0.99$ (Burton & Dahm 2005*b*). Thus, as inverse energy transfer is essential to the development of RTI flows, the nLES method holds the promise of substantially higher-fidelity numerical study of RTI and other buoyancy-driven flows. For a brief summary of the nLES method and its implementation in the NGA code, see the companion paper (Burton 2009). For more extensive discussions of the nLES method, see Burton (2008*a,b*); Burton & Dahm (2005*a,b*).

2.2. *Simulation configuration*

All simulations reported herein were conducted with the nLES method as implemented in the CTR's structured variable-density low Mach-number NGA code. For the details of NGA, see Desjardins *et al.* (2008). All simulations were conducted on a computational domain periodic in the x and z directions, with a no-slip wall condition enforced at the domain boundaries in the inhomogeneous direction y. For the validation simulations at $A = 0.5$, a domain of size $2\pi \times 4\pi \times 2\pi$ was used, with the number of gridpoints $N = 64 \times 128 \times 64$. For the runs at Atwood number $A = 0.94$, a higher aspect-ratio domain of size $2\pi \times 16\pi \times 2\pi$ with gridpoints $N = 64 \times 512 \times 64$ was employed to permit longer time development of the flow. For all runs, an aspect-ratio unity Cartesian mesh was used. Kinematic viscosity was set to $\nu = 3 \times 10^{-4}$ and the Schmidt number

$Sc \equiv \nu/D = 1$, where D is the diffusivity of any passively-transported scalar. The timestep was set to $\Delta t = 5 \times 10^{-4}$, giving at late time a CFL number of ≈ 0.50 for the high Atwood-number runs.

The initial fluid interface was described by a multimode density perturbation function from Dimonte *et al.* (2004), given by

$$h_o(x,y) = \sum_{k_x,k_z} a_k \cos(k_x x)\cos(k_z z) \; + \; b_k \cos(k_x x)\sin(k_z z) + c_k \sin(k_x x)\cos(k_z z) \; + \; d_k \sin(k_x x)\sin(k_z z)\,. \tag{2.1}$$

A short-wavelength broadband perturbation spectrum was selected over a wavemode annulus defined by $k_i \equiv \sqrt{k_x^2 + k_z^2}$ and where $24 \leq |k_i| \leq 31$. Mode amplitudes in equation (2.1) were assigned as a_k, b_k, c_k, $d_k = 1.0 \times 10^{-4}$. In addition, a further divergence-free fluctuation field of $\langle f(x,z)_{rms} \rangle \approx 1.0 \times 10^{-6}$ was added. The configuration allowed for studies of broadband nonlinear mode-coupling in the absence of long-wavelength perturbations that have been shown to substantially alter mixing-layer growth rates.

2.3. *Statistical measures*

The initial validation studies reported here focus on the accuracy with which the nLES method, as described in Burton (2008*a*), captures traditional measures of RTI mixing. To quantify mixing, the local mole fraction of heavy fluid may be defined as

$$X(x,y,z) = \frac{\rho(x,y,z) - \rho_{_L}}{\rho_{_H} - \rho_{_L}}\,, \tag{2.2}$$

where $\rho_{_H}$ and $\rho_{_L}$ are the densities of the heavy and light fluids, respectively. The mole fraction of mixed fluid is then given by

$$X_m(X) \; = 2X\,, \quad \text{if} \;\; X \leq 0.5\,, \tag{2.3}$$

and

$$X_m(X) \; = \; 2(1-X)\,, \quad \text{if} \;\; X > 0.5. \tag{2.4}$$

Using an integral measure, the height of the mixing region can be defined as the thickness of mixed fluid that would result if the heavy and light fluids were perfectly mixed in each $x-z$ plane, as

$$h \equiv \int_{-\infty}^{\infty} X_m(\langle X \rangle)\, dy. \tag{2.5}$$

Bubble and spike heights are calculated using the traditional 1%–99% definitions as

$$\langle X \rangle (y = -h_s^{1\%}) = 1\%\,, \tag{2.6}$$

and

$$\langle X \rangle (y = h_b^{99\%}) = 99\%\,. \tag{2.7}$$

A normalized timescale is given by $t_o = t \,/\, \tau$ where

$$\tau \equiv \left(\frac{\lambda_o}{Ag} \right)^{1/2}, \tag{2.8}$$

and where λ_o is the dominant initial wavelength characterizing the perturbation spectrum at the heavy-light fluid interface. The relative amount of mixed fluid within the mixing layer is traditionally characterized as the ratio of a mixing length to an entrainment

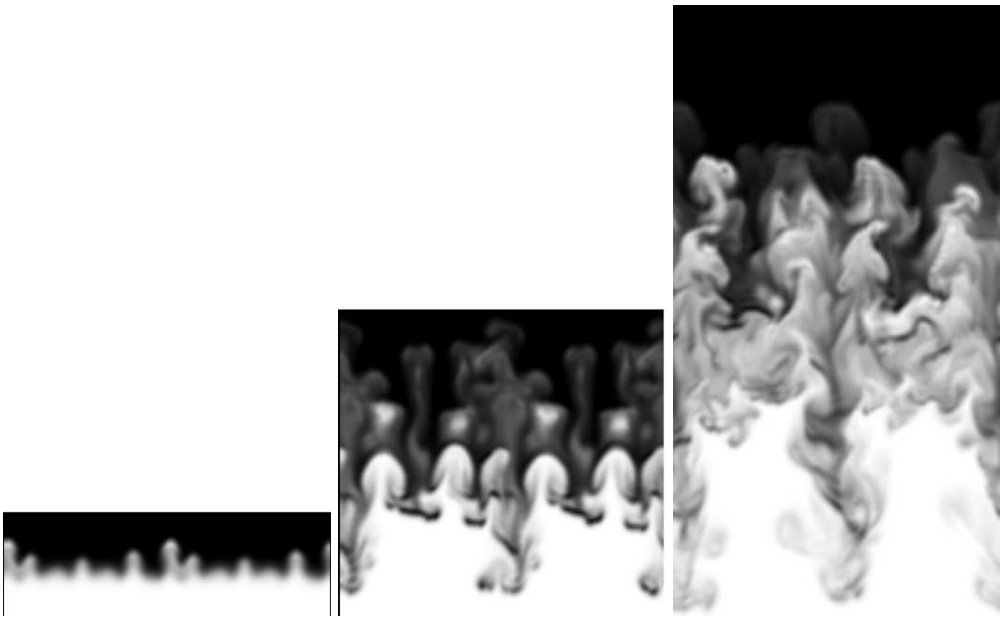

FIGURE 1. Density field at $t/\tau = 2.39$, 4.30, 6.00 for case $A = 0.5$. Grayscale black (*white*) corresponds to heavy (*light*) fluid.

length (Youngs 1991), and is usually given as

$$\Theta \equiv \int_{-\infty}^{\infty} \langle X\,(1 - X)\rangle\, dy \,/\, \int_{-\infty}^{\infty} \langle X\rangle\langle 1 - X\rangle\, dy\,. \tag{2.9}$$

Where $\Theta = 1$, all fluid entrained in the mixing layer has been molecularly mixed, while $\Theta = 0$ corresponds to the immiscible case where the two fluids do not mix. This statistic thus gives an indication of the efficiency of molecular mixing within the mixing layer. Potential energy released in the flow is given as a function of the density difference from the initial condition as

$$PE(t) \equiv \int_V [\,\rho(\mathbf{x}, 0) - \rho(\mathbf{x}, t)\,]\, g\, y\, d^3\mathbf{x}\,. \tag{2.10}$$

The total kinetic energy in the flow is the sum of kinetic energies in the homogeneous and inhomogeneous directions, as

$$KE(t) = KE_{xz}(t) + KE_y(t) = \frac{1}{2}\int_V \rho\,(u^2 + w^2)\, d^3\mathbf{x} + \frac{1}{2}\int_V \rho\, v^2\, d^3\mathbf{x}. \tag{2.11}$$

The ratio of KE/PE thus provides a metric for assessing how dissipative is the mixing process.

3. Results

To validate the implementation of the nLES method in the NGA code, an initial nLES study was conducted of intermediate Atwood-number ($A = 0.5$) RTI mixing. This permitted direct comparison of the nLES results with the "Alpha Group" study of Dimonte *et al.* (2004), the LES study of Cook *et al.* (2004) and the DNS study of Cabot &

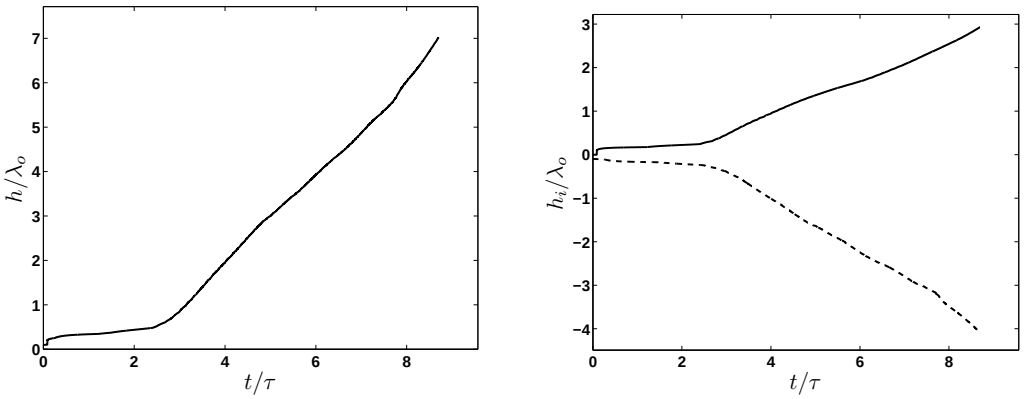

FIGURE 2. *(Left)* Integral mixing layer width h of (2.5) and *(right)* bubble and spike heights h_i of (2.6) and (2.7) for case $A = 0.50$. Ratio $h_s/h_b \approx 1.25$, consistent with prior studies.

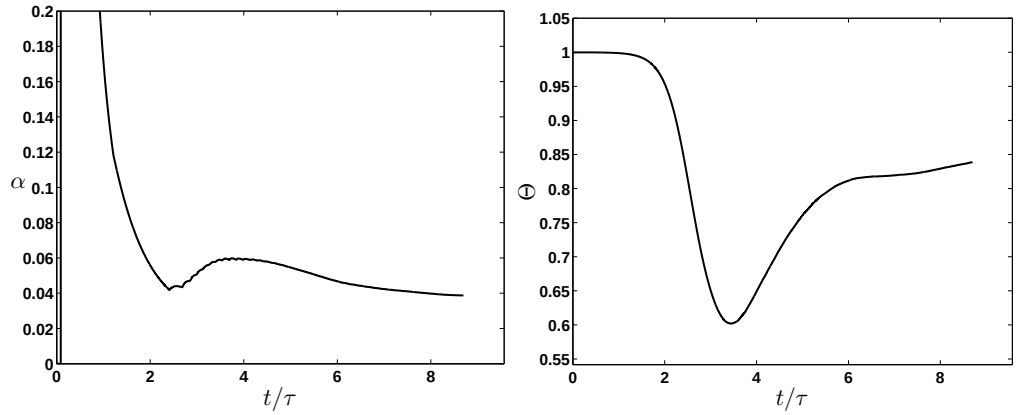

FIGURE 3. Bubble alpha factor α_b *(left)* and mixedness factor Θ *(right)*, showing late-time values of ≈ 0.4 and ≈ 0.83, respectively, for case $A = 0.5$. Neither value has attained its asymptotic limit, indicating that longer-time runs on expanded domains may be required.

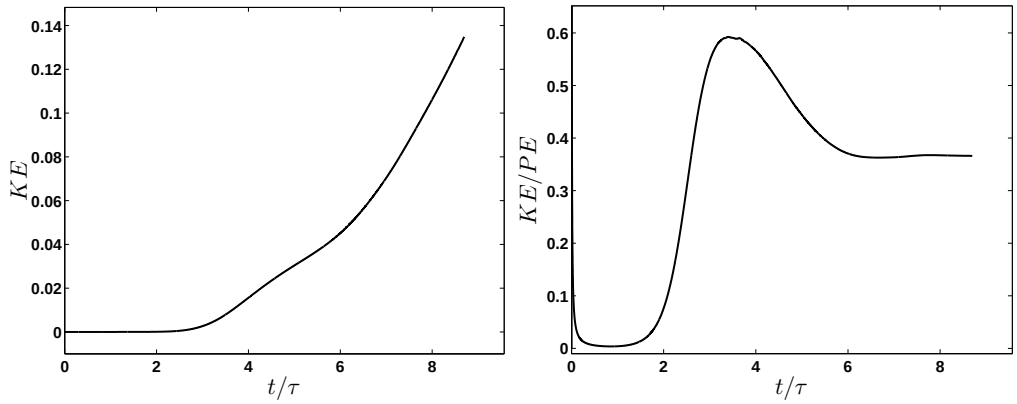

FIGURE 4. *(Left)* Evolution of total kinetic energy (2.11), and *(right)* the ratio of kinetic to released potential energy (2.10) for the case $A = 0.5$. The conversion ratio appears to reach a steady-state value of ≈ 0.385, consistent with previous studies.

Cook (2006). The second part of the study then involved an nLES simulation of three-dimensional RTI mixing at a density ratio of 31 : 1, corresponding to an Atwood number of $A = 0.94$, believed to be the highest density-ratio multimode RTI simulation reported in the literature. As discussed below in Section 4, it is anticipated that significant additional work will be undertaken, beyond the work presented here, to extend the nLES method to higher-fidelity study of RTI mixing.

3.1. *Intermediate Atwood-number* ($A = 0.5$) *study.*

The nLES method and the NGA implementation were first validated in the case of intermediate Atwood number ($A = 0.5$) RTI flow, and compared against results from high-resolution direct numerical and large-eddy simulations of Youngs (1991); Cook *et al.* (2004); Cabot & Cook (2006). The focus is on the accuracy with which the nLES implementation in NGA captures standard statistical measures relating to the mixing layer, such as growth rates and mixing efficiency.

Figure 1 depicts two-dimensional extracts from the density field at three time instants during the simulation at $t/\tau = 2.39$, 4.30 and 6.00. In these graphics, black (white) indicates heavy (light) fluid. Figure 2 *(left)* shows the growth of the mixing-layer width as measured by the integral measure of equation (2.5). Comparing this graphic with Figure 1, it is apparent that the earliest time depicted *(left)* corresponds to the late interpenetration phase, where single-mode growth dominates. The middle and right-hand extracts in Figure 1 correspond to the early and later self-similar growth phase, where nonlinear coupling of modes, reflected in bubbles and spikes, results in the merger of smaller scale structures and alters the growth of the mixing layer.

Figure 2 *(right)* shows the evolution of bubble and spike structure heights, based on a mixing layer metric of $1\%-99\%$ as reflected in (2.6) and (2.7). The ratio of spike to bubble length scales $R = h_s/h_b > 1$ as the density difference between the initial fluids departs from unity. Here, at $A = 0.5$, $R \approx 1.25$ consistent with prior studies at this Atwood number. Figure 3 *(left)* depicts the value of α_b corresponding to the bubble heights as it evolves during the simulation. After the exponential growth predicted for the linear phase, the value for α rapidly settles to a value $0.04 \leq \alpha \leq 0.06$ for the remainder of the simulation. The value has almost relaxed to a constant value at $t/\tau > 8$ of $\alpha \approx 0.041$, higher than the values $0.02 \leq \alpha_b \leq 0.03$ reported by numerical studies of *e.g.,* Cabot & Cook (2006) and others. The nLES result thus falls between values reported in prior numerical studies and the experimental studies that have found $0.05 \leq \alpha \leq 0.08$. As discussed above, this disparity between the experimental and numerical studies may be due in part to numerical dissipation not present in the experimentally-studied RTI flows, as the dissipation results in greater mixing of the two fluids and thus a net reduction in the buoyancy forces driving the growth of the mixing layer. These results suggest that the nLES method may be less dissipative than most other LES approaches that rely on artificial dissipation to stabilize the simulation. Figure 3 *(right)* illustrates the value of the mixing parameter Θ from equation (2.9) during the simulation. As discussed above, Θ gives a relative measure of the efficiency of the mixing layer in reducing density gradients, and hence buoyancy effects, arising from the entrained ambient fluids. By the latest times, the value of $\Theta \approx 0.83$, but has not reached a steady state. The parameter value is, however, close to values reported by other studies (Youngs 1991; Cook *et al.* 2004). Longer time simulations in expanded domains will be necessary to more accurately evaluate the asymptotic value of Θ.

Figure 4 *(left)* depicts the growth of the total kinetic energy in the mixing layer as defined by equation (2.11). Three distinct flow regimes can be identified: *(i)* the linear

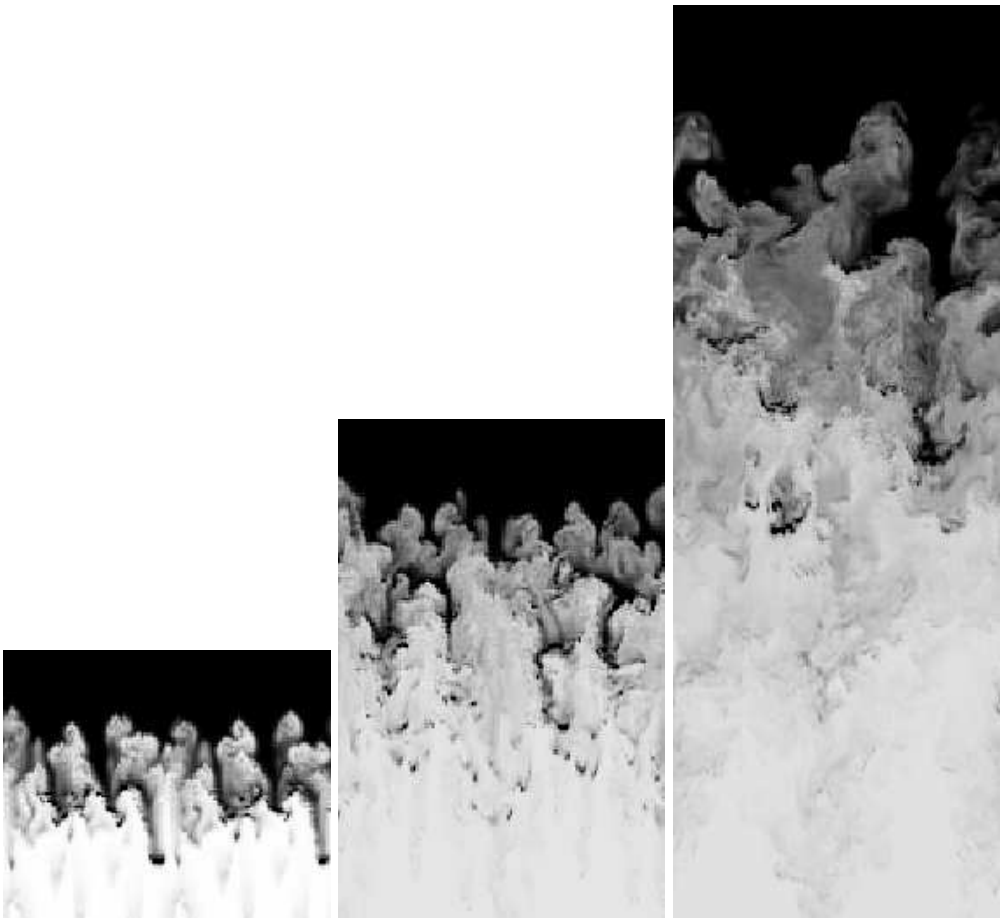

FIGURE 5. Density field at $t/\tau = 6.13$, 10.38, 13.40 for case $A = 0.94$.

regime at $t/\tau \leq 3$ when there is little growth of kinetic energy in the system, *(ii)* an early self-similar phase at $3 \leq t/\tau \leq 6.5$, where kinetic energy is seen growing in the mixing layer as bubble and spike structures merge in a nonlinear fashion, and *(iii)* a later self-similar phase at $t/\tau \geq 6.5$, where an appreciable acceleration can be seen in kinetic energy levels. Figure 4 *(right)* depicts the ratio of total kinetic energy to potential energy liberated by the flow as described by equations (2.10) and (2.11). Previous studies have indicated that the ratio should fall ≈ 0.4 to 0.5. The present study shows the value reaching a steady-state value of ≈ 0.4 as the flow reaches the self-similar state for $t/\tau \geq 6$, in good agreement with prior studies.

3.2. *High Atwood-number* ($A = 0.94$) *study*

Having demonstrated that the nLES implementation in NGA captures important measures of RTI flow at an intermediate Atwood number, we next turn to simulating a much higher Atwood-number problem at $A = 0.94$, corresponding to a density ratio of 31:1. A substantial review of the literature suggests that this configuration may be the highest Atwood-number multimode three-dimensional RTI study yet reported.

As discussed above, given the significantly higher spike velocities, the domain for these

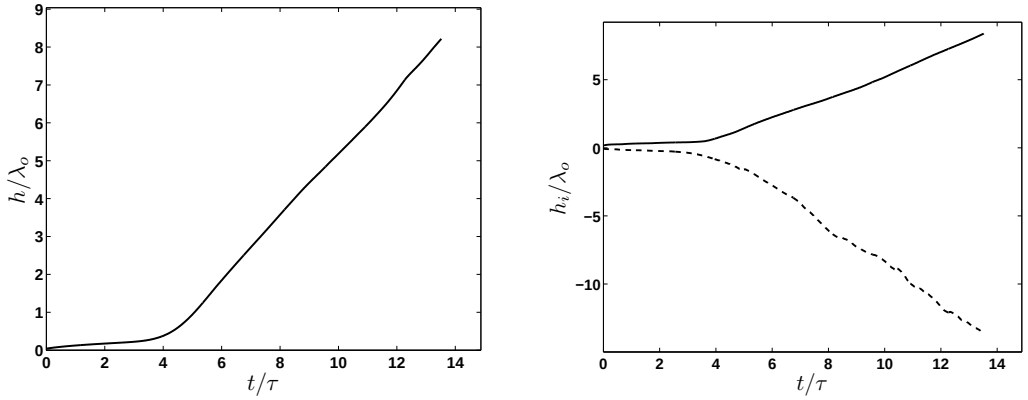

FIGURE 6. *(Left)* Integral mixing layer width h of (2.5) and *(right)* bubble and spike heights h_i of (2.6) and (2.7) for case $A = 0.94$. Ratio $h_s/h_b \approx 1.63$, consistent with prior studies.

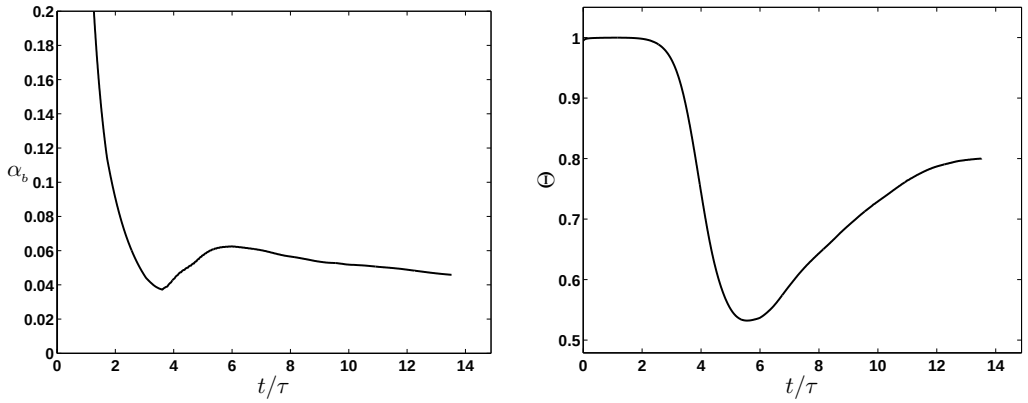

FIGURE 7. For the $A = 0.94$ case, at late time, neither the alpha factor ($\alpha_b \approx 0.48$) *(left)* , nor the mixing factor ($\Theta \approx 0.8$) *(right)* has reached a steady-state value. Late time behavior will be better assessed in future simulations with a larger aspect-ratio (L_y / L_{xz}) domain.

simulations has been expanded somewhat to $L_x \times L_y \times L_z = 2\pi \times 16\pi \times 2\pi$ where $Nx \times Ny \times Nz = 64 \times 256 \times 64$. However, even given the expanded domain and the higher density ratio, the low Mach number approximation of the numerical method remains valid, as the domain remains sufficiently restricted to prevent the appearance of very late-time compressibility effects, such as those reported by Olson & Cook (2007).

Figure 5 illustrates two-dimensional extracts of the density field from the $A = 0.94$ simulation using the nLES method at three time instants, corresponding to $t/\tau = 6.13$, 10.38 and 13.40, i.e., the early, middle and late self-similar stages in the flow evolution *(left right, respectively)*. At the earliest time, prominent bubble and spike structures can be seen soon after the nonlinear coupling of the initial perturbation modes has begun. The extract at $t/\tau = 10.38$ shows the mixing layer at an intermediate time in the self-similar growth period, and indicates that significant bubble merging has already occurred. Finally, the right extract shows the state of the mixing layer immediately before the spikes reach the bottom of the domain. The three graphics illustrate the significant growth of mixing-layer turbulence generated by the coupling of the buoyancy and inertial forces in the nonlinear self-similar regime.

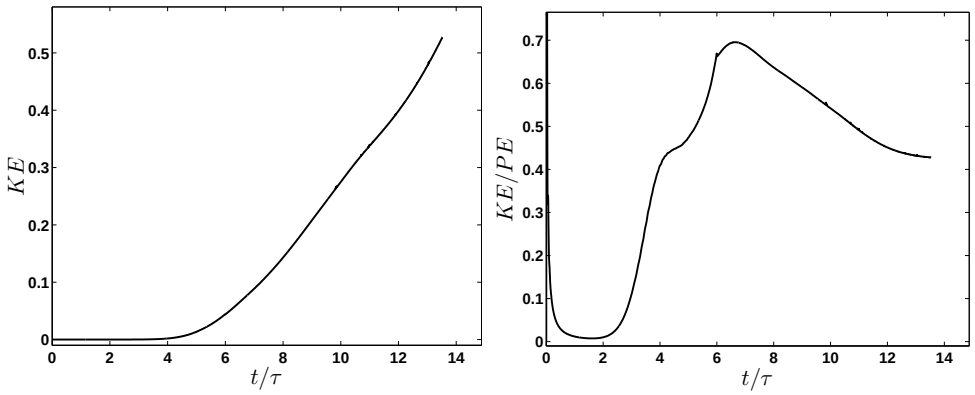

FIGURE 8. *(Left)* Evolution of total kinetic energy (2.11), and *(right)* the ratio of kinetic to released potential energy (2.10) for the case $A = 0.94$. Significantly more kinetic energy is liberated per unit time than in the lower density ratio case, while the conversion ratio appears to be approaching a steady-state value ≈ 0.45, consistent with the $A = 0.5$ case and previous studies.

Figure 6 shows *(left)* the evolution of the integrated mixing-layer width h parameter of equation (2.5), and *(right)* the growth of bubble and spike heights as functions of time. The much larger density ratio gives rise to a much higher rate of spike growth, and the ratio of bubble to spike heights has significantly increased to $R = h_s/h_b \approx 1.8$, reasonably close prior studies. Figure 7 *(left)* shows that the bubble growth rate does not appreciably change over the lower Atwood-number case above, and the parameter α_b shows a late time value of 0.044, although it has not reached a steady-state value before spike contact with the lower boundary. Figure 7 *(right)* shows the evolution of the mixing factor Θ during the simulation. At late time $\Theta \approx 0.8$, suggesting that the entrained fluid is being molecularly mixed at about the same rate as the $A = 0.5$ case, discussed above. At the latest time, however, Θ has not reached a steady-state value. Future studies of this configuration will employ a higher aspect-ratio domain to better evaluate late-time statistical behavior of these quantities.

Finally, Figure 8 shows the evolution of the total kinetic energy *(left)*, and the ratio of kinetic to released potential energy *(right)* as defined in (2.10), during the simulation. Significantly more kinetic energy is released as compared to the $A = 0.50$ case. In addition, at $t/\tau \geq 6.3$ the system shows an accelerated growth of kinetic energy, possibly related to the mixing transition, as discussed in prior studies. The ratio of kinetic to released potential energy appears to have reached a steady value at about that time to $KE/PE \approx 0.43$, in reasonable agreement with prior studies ().

4. Future work

This project is only in its initial stages, with the results reported herein reflecting only a cursory validation of the nLES model implementation in the NGA code. Future work will focus principally on a more complete assessment of nLES model performance in the intermediate and ultra-high Atwood-number regimes. The work will also explore refinements of the nLES method to better recover RTI mixing characteristics. For the high Atwood-number cases, the simulations will likely employ an even higher aspect-ratio computational domain to better assess late-time statistical behavior. Direct comparisons will be made against the dynamic Smagorinsky model (Germano, Piomelli, Moin

& Cabot 1991), in order to better assess the contributions of the nLES subgrid model and backscatter limiter. Work will also focus on better understanding the dynamics of the fully-turbulent mixing layer, with an emphasis on the role of forward and reverse interscale transfer of kinetic and scalar energies. Finally, it hoped that time will permit study of strategies for mitigating RTI mixing, and hence for enhancing TN yields, in ICF applications.

Acknowledgments

The author is grateful to Professors P. Moin and G. Iaccarino for a number of discussions on this project, as well as to G. Blanquart, E. Knudsen, M. Shashank, R. Mittal and C. Schmidt for their help in answering a variety of questions during the implementation of the nLES method into the NGA code.

REFERENCES

Alon, U., Hecht, J., Ofer, D. & Schvarts, D. 1995 Power laws and similarity of Rayleigh-Taylor and Richtmeyer-Meshkov (sic) mixing fronts at all density ratios. *Phys. Rev. Lett.* **74**, 534-537.

Amendt, P., Colvin, J. D., Tipton, R. E. *et al.* 2002 Indirect drive noncryogenic double-shell ignition targets for the National Ignition Facility: design and analysis. *Phys. Plasmas* **9**, 2221-2233.

Blanquart, G., Pepiot-Desjardins, P. & Pitsch, H. 2009 Assessing uncertainties in numerical simulations of simple reacting flows using the FlameMaster code. *Comb. Theory Model.*, in preparation.

Burton, G. C. 2009 Large-eddy simulation of a turbulent helium-air plume using the nLES method. *CTR Annual Briefs 2009.*

Burton, G. C. 2008*a* The nonlinear large-eddy simulation method (nLES) applied to $Sc \approx 1$ and $Sc \gg 1$ passive-scalar mixing. *Phys. Fluids* **20**, 035103.

Burton, G. C. 2008*b* Scalar-energy spectra in simulations of $Sc \gg 1$ mixing by turbulent jets using the nonlinear large-eddy simulation method. *Phys. Fluids* **20**, 071701.

Burton, G. C. & Dahm, W. J. A. 2005*a* Multifractal subgrid-scale modeling for large eddy simulation. Part I: Model development and *a priori* testing. *Phys. Fluids* **17**, 075111.

Burton, G. C. & Dahm, W. J. A. 2005*b* Multifractal subgrid-scale modeling for large eddy simulation. Part II: Backscatter limiting and *a posteriori* evaluation. *Phys. Fluids* **17**, 075112.

Cabot W. & Cook, A. W. 2006 Transition stages of Rayleigh-Taylor instability between miscible fluids. *Nature Physics* **443**, 69-99.

Chandrasekhar, S. 1961 Hydrodynamic and Hydromagnetic Stability. *The Clarenden Press*, New York.

Cook, A. W. & Dimotakis, P. E. 2001 Transition stages of Rayleigh-Taylor instability between miscible fluids. *J. Fluid Mech.* **443**, 69-99.

Cook, A. W., Cabot, W. & Miller, P. L. 2004 The mixing transition in Rayleigh-Taylor instability. *J. Fluid Mech.* **511**, 333-362.

DesJardin, P. E., O'Hern, T. J. & Tieszen, S. R. 2004 Large eddy simulation and experimental measurements of the near-field of a large turbulent helium plume. *Phys. Fluids* **16**, 1866-1883.

Desjardins, O., Blanquart, G., Balarac, G. & Pitsch, H. 2008 High order conservative finite difference scheme for variable density low Mach number turbulent flows. *J. Comp. Phys.* **227**, 71257159.

Dimonte, G., Ramaprabhu, P., Youngs, D. L., Andrews, M. J. & Rosner, R. 2005 Recent advances in the turbulent Rayleigh-Taylor instability. *Phys. Plasmas* **12**, 056301.

Dimonte G. & Schneider, M. 2000 Density ratio dependence of Rayleigh-Taylor mixing for sustained and impulsive accelerations. *Phys. Fluids* **12**, 304-321.

Dimonte, G., Youngs, D. L., Dimits, A. *et al.* 2004 A comparative study of the turbulent Rayleigh-Taylor (RT) instability using high-resolution 3D numerical simulations: The Alpha-Group collaboration. *Phys. Fluids* **16**, 1668-1692.

Germano, M., Piomelli, U., Moin, P. & Cabot, W. H. 1991 A dynamic subgrid-scale eddy viscosity model. *Phys. Fluids* **A 3**, 1760-1765.

Glimm, J., Grove, J. W., Li, X. L., Oh, W. & Sharp, D. H. 2001 A Critical Analysis of Rayleigh-Taylor Growth Rates. *J. Comp. Phys.* **169**, 652-677.

Grinstein, F. F., Margolin, L. G. & Rider, W. J. (eds.) 2007 Implicit large eddy simulation: computing turbulent flow dynamics. *Cambridge University Press*, New York.

Goncharov, V. N. 2002 Analytical model of nonlinear, single-mode, classical Rayleigh-Taylor instability at arbitrary Atwood numbers. *Phys. Rev. Lett.* **88**, 134502.

Layzer, D. 1955 On the instability of superposed fluids in a gravitational field. *Astrophys. J.* **122**, 1-12.

Mikaelian, K.O. 2003 Explicit expressions for the evolution of single-mode Rayleigh-Taylor and Richtmyer-Meshkov instabilites at arbitrary Atwood numbers. *Phys. Rev. E* **67**, 026319.

Olson, B. & Cook A.W. 2007 Rayleigh-Taylor shock waves *Phys. Fluids* **19**, 128108.

Ramaprabhu, P., Dimonte, G. & Andrews, M.J. 2005 A numerical study of the influence of initial perturbations on the turbulent Rayleigh-Taylor instability. *J. Fluid Mech.* **536**, 285-319.

Rayleigh, L. 1883 Investigation of the character of the equilibrium of an incompressible fluid of variable density. *Proc. London Math. Soc.* **14**, 170.

Read, K. I. 1984 Experimental investigation of turbulent mixing by Rayleigh-Taylor instability. *Physica D* **12**, 45-58.

Ristorcelli, J. R. & Clark, T. T. 2004 Rayleigh-Taylor turbulence: self-similar analysis and direct numerical simulation. *J. Fluid Mech.* **507**, 213-253.

Smagorinsky, J. 1963 General circulation experiments with the primitive equations: I. The basic equations. *Mon. Weather Rev.* **91**, 99-164.

Sohn, S. I. 2003 Simple potential flow model of Rayleigh-Taylor and Richtmyer-Meshkov instabilities for all density ratios. *Phys. Rev. E* **67**, 26301.

Taylor, G. I. 1950 The instability of liquid surfaces when accelerated in a direction perpendicular to their planes I. *Proc. R. Soc. London* Ser. A, **201**, 192.

Youngs, D. L. 1991 Three-dimensional numerical simulation of turbulent mixing by Rayleigh-Taylor instability. *Phys. Fluids* **A3**, 1312-1320.

Youngs, D. L. 2009 Application of monotone integrated large eddy simulation to Rayleigh Taylor mixing. *Phi. Trans. R. Soc.* A, **367**, 2971-2983.